DOI: 10.1002/ejic.200700341

Surface-Assisted Synthesis and Behavior of Dimetallic Mixed-Metal Complexes $[M_2Cl_2(\mu\text{-}Cl)_4(CO)_6M'(L)_2]$ (M = Ru, Os; M′ = Fe, Co; L = CH_3CH_2OH, H_2O)

Minna Jakonen,[a] Pipsa Hirva,[a] Taina Nivajärvi,[a] Mirja Kallinen,[a] and Matti Haukka*[a]

Keywords: Ruthenium / Osmium / Cobalt / Iron / Synthesis design

The reductive carbonylation of ruthenium and osmium halides in the presence of cobalt and iron surfaces was studied. In these surface-assisted reactions the metal surface plays an active role in releasing metal ions, which can be used for the in situ synthesis of mixed-metal compounds. A linear, dimetallic, chlorido-bridged, trinuclear complex $[Ru_2Cl_2(\mu\text{-}Cl)_4(CO)_6Co(CH_3CH_2OH)_2]$ was obtained by the interaction between reducing $RuCl_3$ and the cobalt surface. In the reaction the $RuCl_3$ is reduced with carbon monoxide in the presence of a solid cobalt surface in ethanol solution. During the reduction of the $RuCl_3$ the cobalt surface was simultaneously corroded, releasing cobalt cations. In addition to $[Ru_2Cl_2(\mu\text{-}Cl)_4(CO)_6Co(CH_3CH_2OH)_2]$, the reaction also produced other trinuclear complexes and mononuclear products, such as a bent and linear dimetallic, chlorido-bridged complex with the aqua ligand $[Ru_2Cl_2(\mu\text{-}Cl)_4(CO)_6Co(H_2O)_2]$ and ionic $[RuCl_3(CO)_3]_2[Co(H_2O)_6]$. The carbon monoxide reduction of RuI_3 produced the ionic complex $[RuI_3(CO)_3]_2[M'(H_2O)_6]$ (M′ = Fe, Co) in the presence of iron, stainless steel or cobalt. Iodido-bridged trinuclear mixed-metal complexes were not observed. The surface-assisted process proved to be useful with other metal combinations as well. When $RuCl_3$ was replaced with $OsCl_3$, a variety of trinuclear mixed-metal complexes, such as $[Os_2Cl_2(\mu\text{-}Cl)_4(CO)_6Co(CH_3CH_2OH)_2]$ and ionic $[OsCl_3(CO)_3]_2[M(H_2O)_6]$ (M = Fe, Co), were obtained, depending on the metal surface used. Due the lability of the chlorido-bridged trinuclear complexes, the possible decomposition steps of $[M_2Cl_2(\mu\text{-}Cl)_4(CO)_6M'(CH_3CH_2OH)_2]$ (M = Ru, Os; M′ = CO, Fe) were studied computationally, using DFT methods.

Introduction

Sacrificial anodes, most commonly used in corrosion protection,[1] have a variety of applications in synthetic chemistry[2] and in biochemistry.[3] The sacrificial anode donates metal cations in a reaction solution when current is applied to the anode material by an external power source. These released cations can then be used to form organometallic[4] or inorganic complexes,[5] or inorganic nanomaterial.[6] Nanomaterials prepared by means of sacrificial anodes have been used, for example, in catalytic applications[6a] and as the inhibitors in biochemical applications.[6b] Sacrificial anodes are also useful in the applications of organic chemistry:[7] in the polymerisation of organic monomers,[7c] in the preparation of organic compounds and also in electrocarboxylation reactions.[7d,7e] There also exists an example of the electrosynthesis of the Grignard reagent using sacrificial magnesium.[7g] The typical sacrificial anode materials in electrosynthesis are magnesium, zinc, cadmium and aluminum, but examples involving cobalt, copper, nickel, palladium, silver, tin and iron are also available.[4–7]

Although it is known that solid metal surfaces can also participate in the formation of the products without external current, this phenomenon has not been widely used in the synthesis of organometallic compounds. In fact, carbonylmetal chemistry started to develop via the corrosion products formed under harsh conditions.[8] Mond was the first to report the formation of toxic $Ni(CO)_4$ in nickel pipes carrying carbon monoxide gas.[8] In our earlier study, we suggested that the release of the metal from a metal surface by corrosion, without the use of an externally applied current, could be used for the synthesis of other carbonyl-containing metal complexes. Such an approach was applied in the synthesis of mixed-metal trinuclear Ru-Fe-Ru complexes, which were prepared by reducing $RuCl_3$ with carbon monoxide in the presence of an iron-containing metal surface.[9] In this synthesis method, ruthenium(III) salt and the iron-containing metal surface form a metal pair suitable for redox processing, which releases the less noble metal ions from the surface. The metal cations released can then be used in the in situ synthesis of the trinuclear mixed-metal complexes $[Ru_2Cl_2(\mu\text{-}Cl)_4(CO)_6Fe(L)_2]$ (L = H_2O, CH_3CH_2OH) and a mixture of mononuclear ions $[RuCl_3(CO)_3]_2[Fe(H_2O)_6]$. The potential difference between the metal surface and the reducing metal salt determines the rate of dissolution of the metal cations from the metal surface into the reaction system.

[a] University of Joensuu, Department of Chemistry, P. O. Box 111, 80101, Joensuu, Finland
E-mail: matti.haukka@joensuu.fi
Supporting information for this article is available on the WWW under http://www.eurjic.org or from the author.

In the current paper we have extended the use of sacrificial metal surfaces from Ru-Fe systems into the other metal combinations. The goal of the study was to examine whether complexes such as $[Ru_2Cl_2(\mu\text{-}Cl)_4(CO)_6Fe(L)_2]$, shown in Figure 1, could be synthesized using the metal systems Ru-Co, Os-Fe and Os-Co. In addition, the influence of the halide on the reaction progress was studied using $RuCl_3$ and RuI_3 as the reducing components.

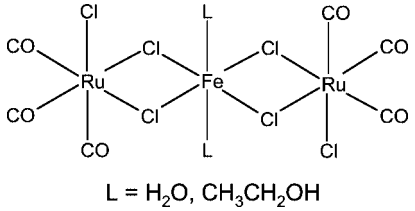

Figure 1. Schematic picture of the chlorido-bridged trinuclear ruthenium-iron complex.[6]

Results and Discussion

The reductive carbonylation of ruthenium(III) trichloride is typically performed in alcohol solutions either under reflux or in high-pressure carbon monoxide. The reduction produces complexes with partially or fully reduced ruthenium centers.[10–15] Normally, the final reduction product is the zero-valent ruthenium cluster $Ru_3(CO)_{12}$ but several compounds containing carbonyl and halide ligands such as $[RuCl_2(CO)_3]_2$ can also be obtained.[11,14,16] Further exposure to carbon monoxide tends to reduce these species eventually to the highly stable $Ru_3(CO)_{12}$ cluster.[15,17] Like $RuCl_3$, the CO reduction of $OsCl_3$ is commonly carried out in alcohol solutions either under reflux or in a pressurized vessel under elevated CO pressure. Such reactions again produce a variety of halide-containing carbonyl products and, finally, $Os_3(CO)_{12}$.[18–20] A different type of surfaces has been used to assist the reduction process. For example, it has been found that reductive carbonylation of silica-supported MCl_3 (M = Ru,Os) produces several halide-containing carbonylmetal(II) compounds as well as the $M_3(CO)_{12}$ cluster.[21]

If metal surfaces are used, this opens up possibilities for synthesizing mixed-metal compounds. For example, if the reductive carbonylation of ruthenium trichloride is carried out in the presence of an iron-containing surface, it acts as a sacrificial source of iron. The active participation of the metal surface permits the formation of mixed-metal products such as trinuclear $[Ru_2Cl_2(\mu\text{-}Cl)_2(CO)_6Fe(L)_2]$ (L = H_2O or CH_3CH_2OH) and also the ionic monomeric $[RuCl_3(CO)_3]_2[Fe(H_2O)_6]$,[6] where the cations and anions are bound together by hydrogen bonds. It is believed that during the reduction of Ru^{3+}, iron from the surface is simultaneously oxidized and released, which leads to the formation of labile trinuclear dimetallic chlorido-bridged compounds $[Ru_2Cl_2(\mu\text{-}Cl)_2(CO)_6Fe(L)_2]$ (L = H_2O or CH_3CH_2OH) with Ru^{2+} and Fe^{2+} centres. The same approach can be applied to other metal combinations using $RuCl_3$ or $OsCl_3$ as the reducing component and iron or cobalt metal as the oxidizing component. The complexes synthesized in this work are summarized in Figure 2.

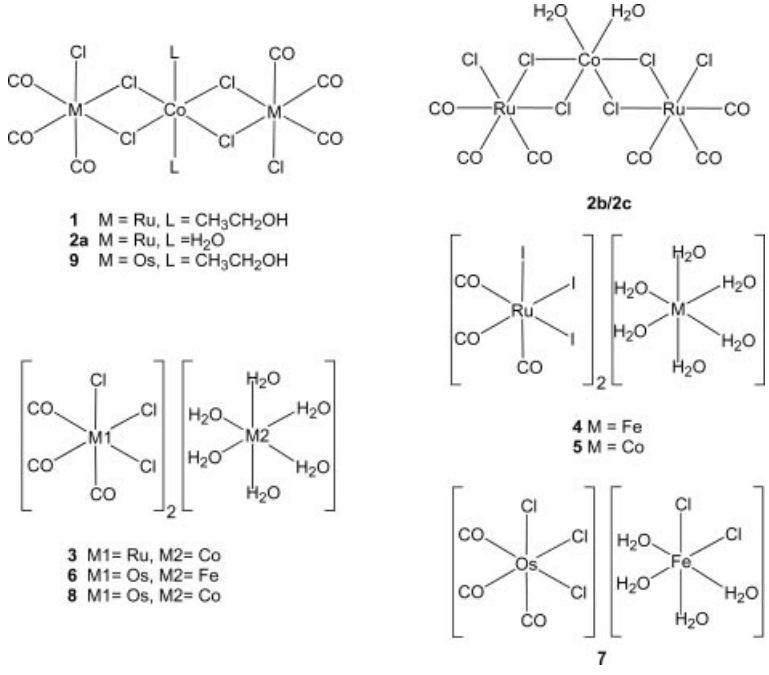

Figure 2. Schematic drawing of the main products involved in the reductive carbonylation reaction of MX_3 in the presence of a sacrificial metal surface.

Corrosion of the metal plate could be detected with all of the metals used as an oxidizing surface. Both iron and cobalt surfaces and also stainless steel do corrode. In the reactions with iron or stainless steel, the initially black reaction solution turned greenish-yellow during the carbonylative reduction of MCl_3. Green or a greenish color was typical for all reactions involving an iron-containing surface, indicating the release of iron ions. When stainless steel was used as the source of iron ions, the type of corrosion produced was pitting, which is typical of metals and metal alloys with a passive oxide layer on their surface.[22] Fairly uniform corrosion was observed when pure metal, iron or cobalt, was used. In a typical reaction with cobalt surface, the reductive carbonylation of $RuCl_3$ produced a blue solution. Again, the metal surface was clearly worn down. A blue coloration indicates the release of cobalt ions into the reaction solution.

Formation of Ruthenium-Cobalt Mixed-Metal Complexes

The carbonylative reduction of $RuCl_3$ in the presence of a cobalt plate consistently produced a mixture of various mixed-metal complexes and mononuclear metal complexes with carbonyl and halide ligands. The ratio of the different products varied with each reaction. Because the yields of the individual products were rather low, single-crystal X-ray diffraction was used as the principal method of analysis. In order to crystallize the products, the reaction solutions were concentrated to dryness and the solid products were recrystallized from dichloromethane by means of slow concentration or by adding hexane to the CH_2Cl_2 solution. In the case of $RuCl_3$ reduction with a cobalt surface, the crystallization produced a mixture of pale pink crystals and colorless crystals. X-ray analysis of the pink crystals revealed trinuclear $[Ru_2Cl_2(\mu\text{-}Cl)_4(CO)_6Co(CH_3CH_2OH)_2]$, as shown in Figure 3.

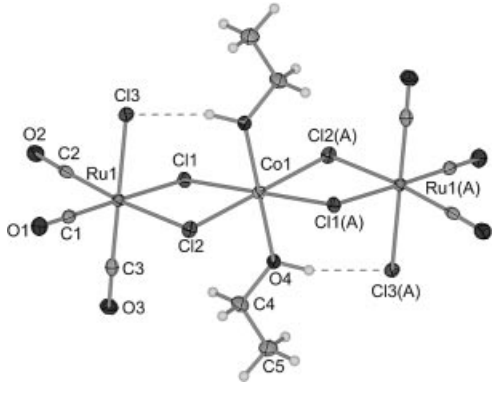

Figure 3. Thermal ellipsoid plot (50% probability level) of $[Ru_2Cl_2(\mu\text{-}Cl)_4(CO)_6Co(CH_3CH_2OH)_2]$ (**1**). Hydrogen bond [Å, °]: O4–H4O 0.95, H4O···Cl3(A) 2.15, O4···Cl3(A) 3.073(2), O4–H4O···Cl3(A) 164.6. Symmetry transformations used to generate equivalent atoms: (A) $-x + 1, -y, -z + 1$.

Structurally, $[Ru_2Cl_2(\mu\text{-}Cl)_4(CO)_6Co(CH_3CH_2OH)_2]$ closely resembles $[Ru_2Cl_2(\mu\text{-}Cl)_4(CO)_6Fe(CH_3CH_2OH)_2]$, as reported earlier.[6] The trinuclear structure is supported by hydrogen bonding between the hydroxy hydrogen atom of the ethanol ligand and the terminal chlorido ligand of the ruthenium moiety. The pink crystals of $[Ru_2Cl_2(\mu\text{-}Cl)_4(CO)_6Co(CH_3CH_2OH)_2]$ could be isolated from the solid product, which was obtained after recrystallization from dichloromethane. The yield of complex **1** was ca. 10–15%. Complex **1** could be obtained both from high-pressure reactions in an autoclave and from low-pressure reactions under reflux. A reasonable yield of the complex **1** permitted further analysis. In order to verify the results, the elemental content of the product was analyzed using both elemental analysis and EDS (Energy Dispersive Spectroscopy). The latter confirmed the presence of cobalt and ruthenium. A pale violet trinuclear complex with aqua ligand, $[Ru_2Cl_2(\mu\text{-}Cl)_4(CO)_6Co(H_2O)_2]$ (**2**), could also be isolated from the product, although the formation of complex **1** seemed to be preferred. The yield of complex **2** remained rather low at ca. 8%. Again, the structural features of $[Ru_2Cl_2(\mu\text{-}Cl)_4(CO)_6Co(H_2O)_2]$ were very similar to $[Ru_2Cl_2(\mu\text{-}Cl)_4(CO)_6Fe(H_2O)_2]$.[6] Two different structures were found: linear **2a**, presented in Figure 4, and bent **2b**, presented in Figure 5. In both structures the intramolecular hydrogen bonds between the coordinated water molecule and the terminal chlorido ligand further support the trinuclear arrangement of the metal atoms. It was found that the formation of the bent type of isomer **2b** was preferred over linear **2a** when the cobalt plate was replaced by cobalt powder. Such an observation may suggest that the morphology of the surface plays an important role in the formation of trinuclear mixed-metal products.

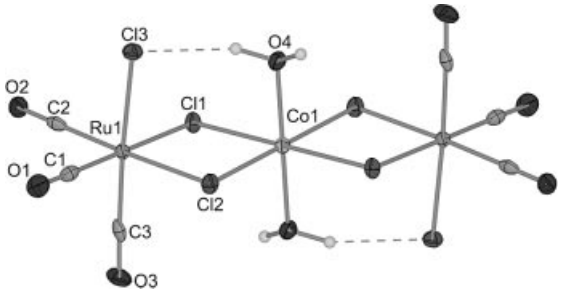

Figure 4. Thermal ellipsoid plot (50% probability level) of $OsCl_2(CO)_3(H_2O)$ (**2a**). Hydrogen bonds [Å, °]: O4–H4 0.98, H4···Cl3 2.30, O4···Cl3 3.242(3), O4–H4···Cl2(A) 161.8.

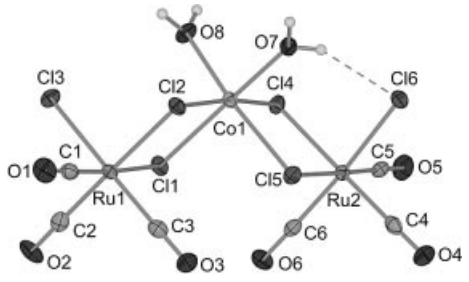

Figure 5. Thermal ellipsoid plot (50% probability level) of the bent $[Ru_2Cl_2(\mu\text{-}Cl)_4(CO)_6Co(H_2O)_2]$ (**2b**), crystallized in the triclinic space group $P\bar{1}$. Hydrogen bond [Å, °]: O7–H7A 0.79, H7A···O2 2.59, O7···O2 3.187(3), O7–H7A···O2 133.2.

The chlorido-bridged trinuclear mixed-metal complexes of types **1** and **2** are labile and sensitive towards moisture. Previous results suggest that the exposure of $[Ru_2Cl_2(\mu\text{-}Cl)_4(CO)_6Fe(CH_3CH_2OH)_2]$ to moisture leads first to ligand exchange on the central metal atom and then to the formation of $[Ru_2Cl_2(\mu\text{-}Cl)_4(CO)_6Fe(H_2O)_2]$. Additional exposure to moisture finally breaks down the chlorido bridges and pulls the metal atoms apart, yielding ionic $[Ru(CO)_3Cl_3]_2[Fe(H_2O)_6]$.[6] Similar behavior was also observed with complex **1**. As in the case of the $RuCl_3$/Fe reaction, the $RuCl_3$/Co reaction produced an ionic decomposition product, $[Ru(CO)_3Cl_3]_2[Co(H_2O)_6]$ (**3**), with variable ratios (Figure 6).

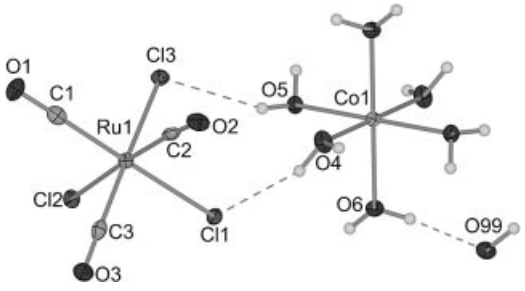

Figure 6. Thermal ellipsoid plot (50% probability level) of $[RuCl_3(CO)_3]_2[Co(H_2O)_6]\cdot 2(H_2O)$ (**3**). The symmetry-related water molecule is not shown. Hydrogen bonds [Å, °]: O4–H4A 0.85, H4A···Cl1 2.36, O4···Cl1 3.140(2), O4–H4A···Cl1 152.8, O5–H5B 0.84, H5B···Cl3 2.44, O5···Cl3 3.220(2), O5–H5B···Cl3 153.8, O6–H6B 0.84, H6B···O99 1.88, O6···O99 2.716(2), O6–H6B···O99 173.3.

Compared to $[Ru_2Cl_2(\mu\text{-}Cl)_4(CO)_6Fe(CH_3CH_2OH)_2]$ and $[Ru_2Cl_2(\mu\text{-}Cl)_4(CO)_6Fe(H_2O)_2]$, the decomposition of complexes **1** and **2** into the ionic product **3** seems to be slightly slower. For example, complex **1** can be stored in air much longer than the corresponding iron compound without severe decomposition.

In addition to complexes **1**, **2**, and **3**, crystallographic analysis of the reaction products obtained after the reduction of $RuCl_3$ in the presence of cobalt revealed other types of mononuclear products as well such as neutral $RuCl_2(H_2O)(CO)_3$ and $CoCl_2(H_2O)_4$, which could be identified by means of single-crystal X-ray diffraction. This suggests that an alternative decomposition route for trinuclear Ru-Co-Ru may also be possible. The formation of corresponding neutral mononuclear species has been observed in $RuCl_3$/Fe systems earlier, which means that a similar alternative route also exists in the case of $RuCl_3$/Co systems. However, it should be mentioned that, according to the very low yields of the neutral products, this route seems not to be very feasible. Actually, neutral products such as $RuCl_2(H_2O)(CO)_3$ were found only occasionally in some of the reaction products. Each reaction was repeated several times, and the main decomposition product was always found to be ionic $[Ru(CO)_3Cl_3]_2[Co(H_2O)_6]$.

The product distribution of the carbonylative reduction of $RuCl_3$ depends strongly on the reaction conditions. If the reaction is carried out without metal surfaces and if the CO pressure is high enough (> 20 bar) and the reaction time long enough (> 17 h), the dominating carbonylation product is zero-valent, fully carbonylated and reduced $Ru_3(CO)_{12}$. This seems to be true for both reactions, with or without the presence of the solid metal surface. The solvent also has an effect on the progression of the reaction and on the products formed during the reduction. If the alcohol solvent is replaced with water, the final carbonylation product is polymeric $[Ru(CO)_4]_n$.[23] However, the presence of the metal surface tends to favor the partially reduced and carbonylated ruthenium species. If $RuCl_3$ was simply heated under reflux in ethanol and in a CO flow in the presence of an iron or cobalt plate (17 h), $Ru_3(CO)_{12}$ was not detected at all. After 3 h of reaction with 20 bar of CO, the cluster product was still not observable. Increasing the reaction temperature from 125 °C to 150 °C led to the formation of $Ru_3(CO)_{12}$ after only 3 h of reaction with 20 bar of carbon monoxide, but under these conditions $Ru_3(CO)_{12}$ was only a minor product. At 50 bar of CO, ≥ 125 °C and ≥ 3 h reaction times with or without the presence of a metal surface, the principal product was an $Ru_3(CO)_{12}$ cluster. Cluster formation under similar conditions without metal surface is well known and reported by Bruce et al.[24] Nevertheless, it should be noted that partially carbonylated species can still be found even with elevated pressures (50 bar) and long reaction times (17–20 h), where $Ru_3(CO)_{12}$ is already the main product, including in reactions with a metal surface. It seems likely that products with partially reduced ruthenium centres $[Ru_2Cl_2(\mu\text{-}Cl)_4(CO)_6M(L)_2]$, and $[Ru(CO)_3Cl_3]_2[M(H_2O)_6]$ (M = Fe, Co and L = H_2O, CH_3CH_2OH) are stable enough to interfere with the reduction of ruthenium in the zero-valent state.

From the synthetic point of view, the formation of an unpredictable mixture of products is the main setback, which complicates the use of metal surfaces for synthetic purposes. The yields of the most interesting products, the mixed-metal trinuclear $[Ru_2Cl_2(\mu\text{-}Cl)_4(CO)_6Co(L)_2]$ complexes, consistently remained rather low at around 8–15%. This is mainly due to the lability of the trinuclear compounds in the presence of moisture. However, compared to its Ru-Fe-Ru equivalent, $[Ru_2Cl_2(\mu\text{-}Cl)_4(CO)_6Co(L)_2]$ can certainly be synthesized with better reproducibility and enhanced yields.

The reaction products **1**–**3**, which were obtained with adequate yields, were also analysed using IR spectroscopy. The common feature of all these compounds is that the arrangement of the carbonyl ligands around the ruthenium center is very similar in all of them. The facial arrangement of the CO ligands in each compound gives a ν(CO) pattern with two strong bands: a sharp band at higher wavenumbers around 2140–2145 cm^{-1} and a broad- or double-headed one at lower wavenumbers at ca. 2055–2065 cm^{-1}. Two pairs of ν(CO) signals were found at 2143 cm^{-1} and 2077 cm^{-1} in the CH_2Cl_2 solution immediately after reaction, when ethanol is evaporated from the Ru-Co reaction solution and the solid material is dissolved in CH_2Cl_2. Typically, the higher band was sharp and the lower band much broader. The result closely resembles those found in reactions conducted with iron-containing surfaces, where the

corresponding signals have been reported to be at 2143 cm^{-1} and 2078 cm^{-1}.[6]

ATR-IR (Attenuated Total Reflectance IR) measurements were performed for the chlorido-bridged Ru-Co-Ru complexes **1** and **2**, and for ionic **3**. In the IR measurements of the reaction solutions different complexes could not be assigned, but with the ATR technique the complexes could be identified. In the case of the ATR measurements two bands were detected again, and as with the FTIR spectra the peak at the higher wavenumber was once again strong and rather sharp. The lower peak was double-headed and actually a combination of two peaks. In the spectrum of complex **1** the highest signal is at the wavenumber 2137 cm^{-1}, while the lower band has two peaks, at 2075 and 2054 cm^{-1}. Similar patterns can be found also in the spectra of the compounds **2** and **3** with the wavenumbers 2135, 2070, and 2054 cm^{-1} for **2** and 2139, 2075, and 2056 cm^{-1} for **3**.

The Effect of the Halide in the Reducing Salt

In order to study the role of the halide in the reducing salt, the $RuCl_3$ was replaced with RuI_3. Otherwise, the reductive carbonylation reaction with cobalt or iron surfaces was carried out under conditions similar to those used for a typical $RuCl_3$ reduction (20 bar of CO, 125 °C, 3 h). Again, the release of iron and cobalt cations was observed in the reaction. The most noticeable feature of these reactions was the absence of halide-bridged trinuclear mixed-metal products. They were detected in reduction reactions with either of the metals (Fe, Co) used. This may indicate that the trinuclear iodido-bridged products are less stable than their chlorido-bridged analogues. The reaction with RuI_3 produced variable amounts of $[RuI_3(CO)_3]_2[Fe(H_2O)_6]$ (**4**), $[RuI_3(CO)_3]_2[Co(H_2O)_6]$ (**5**), $[RuI_2(CO)_3]_2$ (**11**) and $Ru(CO)_4I_2$ (**12**), which were characterized by single-crystal X-ray diffraction. Structurally, compounds **4** and **5** are isostructural with the corresponding complex **3** formed in the reduction reactions of $RuCl_3$. The structures of **4**, **11** and **12** are shown in Figures 7, 8, and 9.

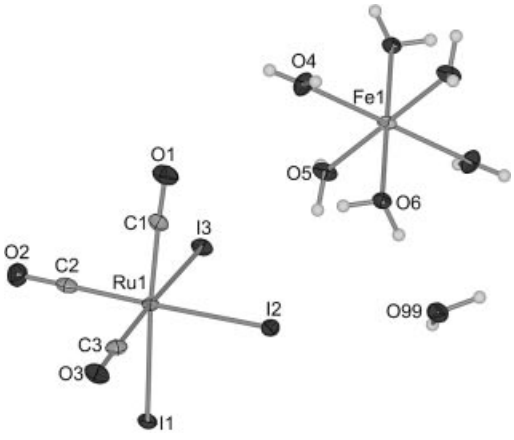

Figure 7. Thermal ellipsoid plot (50% probability level) of $[RuI_3(CO)_3]_2[Fe(H_2O)_6]\cdot 2(H_2O)$ (**4**). The symmetry-related second $[RuI_3(CO)_3]^-$ anion and the solvent water molecule are not shown. Hydrogen bonds [Å, °]: O4–H4A 0.78, H4A···O1 3.14, O4···O1 3.534(6), O4–H4A···O1 114.2, O5–H5A 0.81, H5A···I2 2.83, O5···I2 3.602(4), O5–H5A···I2 159.3, O5–H5B 0.79, H5B···I3 3.32, O5···I3 3.721(4), O5–H5B···I3 176.1, O6–H6A 0.85, H6A···O(99) 1.90, O6···O99 2.752(5), O6–H6A···O99 176.1.

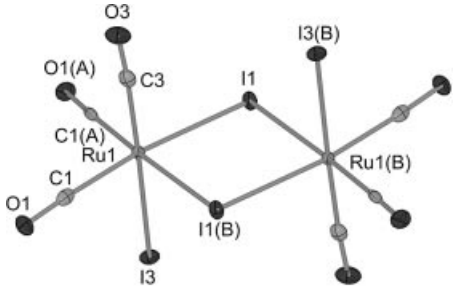

Figure 8. Thermal ellipsoid plot (50% probability level) of $[RuI_2(CO)_3]_2$ (**11**). Symmetry transformations were used to generate equivalent atoms: (A) $x, -y, z$; (B) $-x, -y, -z + 1$.

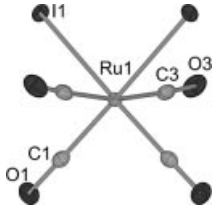

Figure 9. Thermal ellipsoid plot (50% probability level) of $RuI_2(CO)_4$ (**12**).

Another difference between the RuI_3 reactions and the reduction reactions of $RuCl_3$ was the strongly decreased formation of $Ru_3(CO)_{12}$. In fact, this was not observed at all even at higher pressures (50 bar) and with long reaction times (20 h). In the reactions under 50 bar pressure of carbon monoxide, the reduction reaction (125 °C, 3–20 h) produced $[RuI_2(CO)_3]_2$ (**11**), presented in Figure 8. The $RuI_2(CO)_4$ (**12**) presented in Figure 9 was found only in the reactions with iodine salt, while no equivalent chloride product was observed in the $RuCl_3$ reactions.

The Carbon Monoxide Reduction of $OsCl_3$ in the Presence of a Sacrificial Metal Surface

The carbonylative reduction of $OsCl_3$ follows the general lines of the reduction of $RuCl_3$. The final reduction product is the zero-valent cluster $Os_3(CO)_{12}$, especially under high pressures.[18–21] In the current study, the reduction reactions were performed in an alcohol solution either under reflux with a CO stream passing through the reaction solution or in a pressurized autoclave. In both of the reaction setups a sacrificial metal plate (stainless steel, Fe or Co) was added to the system. During the reduction reaction the colour of the solution turned from black to brownish-yellow when an iron-containing plate was used, and greenish-blue when cobalt was used. In all of the osmium reactions, either under reflux or in an autoclave, a dark brown-grey metallic powder was formed. The powder was removed from the solution by filtering prior to crystallization of the carbon-

ylation products. The metallic powder material was characterized with the aid of EDS measurements, which confirmed that the solid material consisted mainly of metallic osmium. The filtrate was analyzed after it had been concentrated and redissolved in dichloromethane. IR analysis revealed two peaks in the ν(CO) region with both Os-Fe and Os-Co systems. In solutions containing Os-Fe, the higher band at 2135 cm^{-1} was again sharp and the lower one at 2058 cm^{-1} was broader. A similar pattern was also found with the Os-Co reaction solution, which produced corresponding peaks at 2135 cm^{-1} and 2054 cm^{-1}. In comparison with the Ru-Fe/Co bands, the Os-Fe/Co bands shifted towards lower wavenumbers, but the shape and relative intensities of the bands remained the same in all cases.

The crystallization of the osmium-iron and osmium-cobalt products was much more difficult than that of the ruthenium-iron or, in particular, of the ruthenium-cobalt products. In consequence, the final yields of the separated products remained very low. This also prevented further analysis of the isolated products. Crystallization was performed according to the same procedure as for the ruthenium reactions. Only the mononuclear products could be isolated and characterized from the Os-Fe reactions. Ionic $[OsCl_3(CO)_3]_2[Fe(H_2O)_6]$ (**6**) is the structural equivalent of $[RuCl_3(CO)_3]_2[Co(H_2O)_6]$ (**3**) and another ionic product $[OsCl_3(CO)_3][FeCl_2(H_2O)_4]$ (**7**). In **7**, the osmium atom is in an oxidation state of 2+ and the iron atom is in an oxidation state of 3+. However, this minor product was obtained only from one reaction. The equivalent of complex **7** was observed neither in any of the Ru-Co or Ru-Fe reactions nor in the Os-Co reactions. Another mononuclear reduction product of $OsCl_3$ with no ruthenium counterpart was $OsCl_2(CO)_3(CH_3CH_2OH)$ (**10**). This product was also a minor product found only from one reaction. The solid-state structure of **10** consists of two osmium moieties bound together with a hydrogen bond (Figure 10).

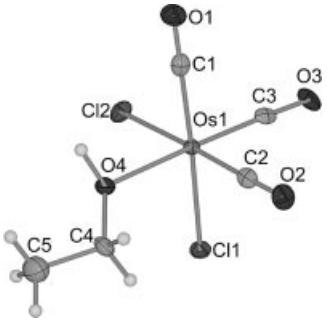

Figure 10. Thermal ellipsoid plot (50% probability level) of $OsCl_2(CO)_3(EtOH)$ (**10**).

From the osmium-cobalt reaction, $[OsCl_3(CO)_3]_2[Co(H_2O)_6]$ (**8**) could be isolated and characterized by means of the single-crystal X-ray diffraction (Figure 11). ATR measurements of the analysed complex **8a** revealed a pattern of signals that was similar to those found by means of the measurements of the Ru-Co complexes **1**, **2** and **3**. The higher band was again sharp at a wavenumber of 2126 cm^{-1}, and the lower peak was a combination of two peaks at wavenumbers of 2043 cm^{-1} and 2024 cm^{-1}. Compared with the ATR-IR spectra of ruthenium analogues, the signals are shifted to a lower wavenumber, but the shape and intensity of the signals remained the same.

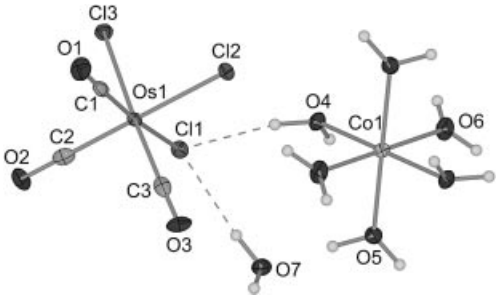

Figure 11. Thermal ellipsoid plot (50% probability level) of $[OsCl_3(CO)_3]_2[Co(H_2O)_6]\cdot 2(H_2O)$ (**8a**). The symmetry-related second $[OsCl_3(CO)_3]^-$ anion and the second water molecule are not shown. Hydrogen bonds [Å, °]: O4–H4B 0.99, H4B···Cl1 2.27, O4···Cl1 3.216(3), O4–H4B···Cl(1) 159.9, O7(A)–H7(A) 0.94, H7(A)···Cl1 2.36, O7(A)···Cl1 3.292(3), O7–H7(A)···Cl1 173.5.

An ethanol-containing trinuclear complex with chlorido bridges, $[Os_2Cl_2(\mu\text{-}Cl)_4(CO)_6Co(CH_3CH_2OH)_2]$ (**9**), could also be found in the osmium-cobalt reactions. Structurally, **9** is similar to $[Ru_2Cl_2(\mu\text{-}Cl)_4(CO)_6M(CH_3CH_2OH)_2]$ (M = Fe, Co) (Figure 12).

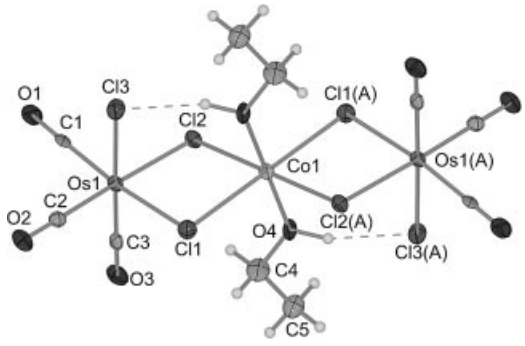

Figure 12. Thermal ellipsoid plot (50% probability level) of $[Os_2Cl_2(\mu\text{-}Cl)_4(CO)_6Co(CH_3CH_2OH)_2]$ (**9**). Hydrogen bond [Å, °]: O4–H4 0.95, H4···Cl3(A) 2.15, O4···Cl3(A) 3.072(6), O4–H4···Cl3(A) 162.4.

The formation of trinuclear halide-bridged compounds is not as favorable with Os/Fe and Os/Co metal pairs as it is with the Ru/Co pair. Complex **9** was separated in some of the reactions, but significantly more rarely than with the ruthenium analogue **1**. Although Os/Co trinuclear halide-bridged complexes were rare and Os/Fe analogues were not detected during our study, this does not necessarily mean that such a compound cannot be formed at all. Such a product may either be less stable, or the absence of these complexes may simply be due to the fact that the reaction setup as it now exists is unsuitable for osmium reactions. In addition, it can be stated that control of the products in the $OsCl_3$ reactions was undoubtedly more difficult than with $RuCl_3$.

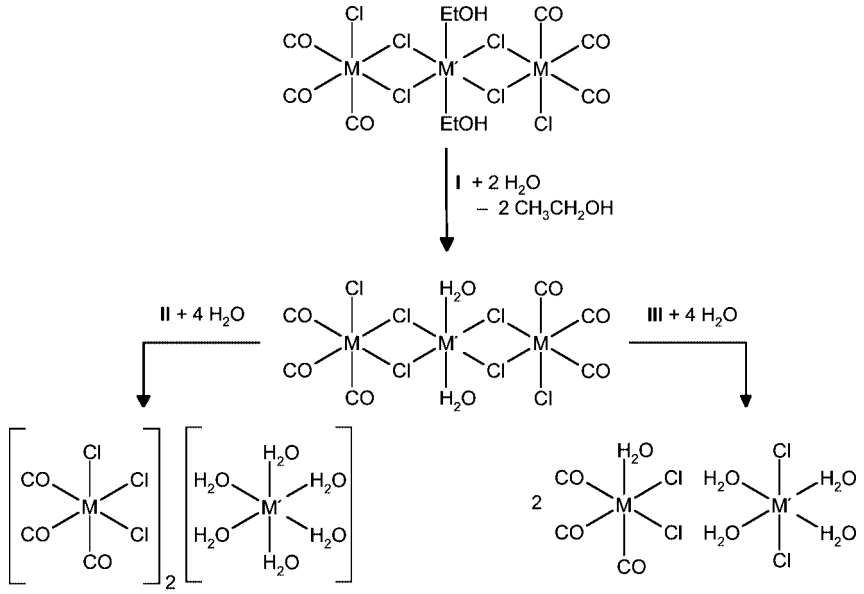

Scheme 1. Decomposition steps of μ-Cl dimetallic trinuclear complexes.

Stability of the Trinuclear Complexes

Computational work was done to investigate the stability of the complexes by means of their relative energies. In our previous study we investigated[6] the decomposition path of $[Ru_2Cl_2(\mu\text{-}Cl)_4(CO)_6Fe(CH_3CH_2OH)_2]$. The presence of water launches the decomposition of the halide-bridged trinuclear mixed-metal complexes. The decomposition pathway proceeds by the replacement of the ethanol ligands with water and the formation of $[Ru_2Cl_2(\mu\text{-}Cl)_4(CO)_6Fe(H_2O)_2]$ and its eventual decomposition into the mononuclear products $[RuCl_3(CO)_3][Fe(H_2O)_6]$, $[RuCl_2(CO)_3(H_2O)]$ and $[FeCl_2(H_2O)_4]$. In the current study we have investigated a similar decomposition route for the Ru/Co, Os/Fe and Os/Co systems by using computational DFT methods. The decomposition steps involved are summarized in Scheme 1 and in Table 1.

Table 1. Calculated DFT energies of the decomposition routes presented in Scheme 1. Values in bold are taken from ref.[9]

M	M′	E_I (kJ/mol)	E_{II} (kJ/mol)	E_{III} (kJ/mol)
Ru	**Fe**	**–34**	**–325**	**67**
Ru	Co	–31	–287	68
Os	Fe	–33	–327	92
Os	Co	–29	–287	106

The first step in the decomposition of $[M_2Cl_2(\mu\text{-}Cl)_4(CO)_6M'(CH_3CH_2OH)_2]$, the replacement of CH_3CH_2OH with H_2O at the bridging metal atom (either Fe or Co), is favourable with all of the metal combinations. The reaction energy of the ligand exchange is around –30 kJ/mol. The two possible structural isomers of $[M_2Cl_2(\mu\text{-}Cl)_4(CO)_6M'(H_2O)_2]$, bent and linear, are energetically very similar to each other, which explains the co-existence of both structures. The relative energy between the bent and linear isomers for all the metal combinations is ca. 4 kJ/mol.

The decomposition of $[M_2Cl_2(\mu\text{-}Cl)_4(CO)_6M'(H_2O)_2]$ can follow two different main steps (steps **II** and **III** in Scheme 1). The addition of 4 equiv. of H_2O breaks down the chlorido bridges and results in ionic $[MCl_3(CO)_3]_2[M'(H_2O)_6]$ or $[MCl_2(CO)_3(H_2O)]$ and $[M'Cl_2(H_2O)_4]$. According to our calculations, the relative energies of the decomposition products formed along step **II** are around 300 kJ/mol more favourable than for the trinuclear chlorido-bridged complexes. The result agrees well with the experimental results: $[MCl_3(CO)_3]_2[M'(H_2O)_6]$ is the favoured product, although $[MCl_2(CO)_3(H_2O)]$ and $[M'Cl_2(H_2O)_4]$ have been observed from reactions of the ruthenium-cobalt system. It also seems that decomposition step **III** is around 40 kJ/mol more favourable with iron than with cobalt, which is also consistent with experimental observations. According to our calculations, in $M'Cl_2(H_2O)_4$ the most favourable isomer is the *trans*(Cl) structure when the metal atom is iron and the *cis*(Cl) structure when the metal atom is cobalt, although the energy difference between the isomers is less than 5 kJ/mol for both metal chlorides. There are no notable differences in the calculation results between the Ru-Fe, Ru-Co, Os-Fe and Os-Co systems.

Conclusions

The reductive carbonylation of MCl_3 (M = Ru or Os) in the presence of a metal surface (Fe or Co) produces a variety of mixed-metal products, whose components originate from the reducing MCl_3 and from the oxidizing surface. The metal ions released from the oxidizing surface can be used for an in situ complex formation. Although this approach produces a mixture of products, it nevertheless provides a useful method for synthesizing trinuclear mixed-metal compounds of the type $[M_2Cl_2(\mu\text{-}Cl)_4(CO)_6M'(L)_2]$

(M = Ru, Os; M′ = Fe, Co; L = CH_3CH_2OH, H_2O). For example, a synthesis of $[Ru_2Cl_2(\mu\text{-}Cl)_4(CO)_6Co(CH_3CH_2OH)_2]$ can be repeated with moderate yields. The main problem in the production of $[M_2Cl_2(\mu\text{-}Cl)_4(CO)_6M'(CH_3CH_2OH)_2]$ is that this can be decomposed relatively easily by moisture into mononuclear species such as $[MCl_3(CO)_3]_2[M'(H_2O)_6]$, $[MCl_2(CO)_3(H_2O)]$ and $[M'Cl_2(H_2O)_4]$.

Mechanistically, the reductive carbonylation of MCl_3 (M = Ru or Os) in the presence of a metal surface (Fe or Co) follows similar reaction pathways regardless of the reducing metal halide and oxidizing metal surface used. Further, the decomposition of the mixed-metal trinuclear $[M_2Cl_2(\mu\text{-}Cl)_4(CO)_6M'(L)_2]$ by moisture is similar in all studied cases. In the case of $[M_2Cl_2(\mu\text{-}Cl)_4(CO)_6M'(CH_3CH_2OH)_2]$, the first step in the decomposition is the replacement of the ethanol ligands by water at the central metal atom (Fe or Co). This is followed by cleavage of the chlorido bridges and the formation of mononuclear products. Energetically, the most favorable decomposition products are ionic compounds of the type $[MCl_3(CO)_3]_2[M'(H_2O)_6]$.

The iodide salt RuI_3 can be used instead of $RuCl_3$ in the preparation of ionic products, but no trinuclear compounds of the type $[M_2I_2(\mu\text{-}I)_4(CO)_6M'(L)_2]$ have been obtained so far. This is probably due to the poorer stability of $[M_2I_2(\mu\text{-}I)_4(CO)_6M'(L)_2]$ compared to its chlorido equivalents.

Experimental Section

Materials and Measurements: $RuCl_3{\cdot}x(H_2O)$ (99.9%) was purchased from Alfa Aesar, $OsCl_3{\cdot}x(H_2O)$ from Sigma Aldrich and RuI_3 from Strem. The metal plates Co (99.9%, CO000279/3), Fe (99.5%, FE000400/11) and stainless steel were from GoodFellow. The cobalt powder (99.995%) was a product from Aldrich. MeOH (p.a.) and CH_2Cl_2 (p.a.) were obtained from Fluka, hexane (p.a.) from Merck, and ethanol (99.5%) from Primalco. The carbon monoxide (98%) used in reactions was purchased from Messer and AGA. The FTIR spectra were measured with a Nicolet Magna IR Spectrometer 750, and ATR-IR measurements were performed using an FTS 7000 Series DIGILAB FTIR spectrometer equipped with a UMA 600 DIGILAB microscope. CE Instruments EA 110 CHNS-O was used in the elemental analyses. Qualitative analyses of cobalt and osmium were conducted using an FE-SEM Hitachi S-4800 Scanning Electron Microscope equipped with a Norman System Six EDS.

Syntheses

High-Pressure Reactions: Metal trichloride [$RuCl_3{\cdot}x(H_2O)$, RuI_3 or $OsCl_3{\cdot}x(H_2O)$] reduction reactions were carried out in a Berghof autoclave equipped with a PTF liner. The solid metals (Co, Fe, stainless steel, 7×7 mm $\times$ 0.02–0.03 mm or 50 mg of cobalt powder) and 100 mg of metal trichloride reagent were placed in the liner together with 4 mL of ethanol. The autoclave was pressurized with 10, 20 or 50 bar of carbon monoxide (in a typical reaction the CO pressure was 20 bar), quickly heated to 125 °C, and maintained at that temperature for 3 h. After the reaction, the autoclave was cooled in an ice bath. The reaction solution was filtered to remove any possible solid metallic precipitations formed during the reaction. The filtrate was concentrated to dryness and the solid residue dissolved in CH_2Cl_2. Crystallization was performed using the CH_2Cl_2 solution by slow concentration or by adding hexane to the CH_2Cl_2 solution.

Reactions under Reflux: Metal trichloride [$RuCl_3{\cdot}n(H_2O)$ or $OsCl_3{\cdot}3(H_2O)$, 250 mg] was placed in a two-necked round-bottom vessel with a metal plate (Co or Fe or stainless steel, 7×7 mm). MCl_3 was diluted in 40 mL of ethanol and the reaction mixture was refluxed in a carbon monoxide stream for 17–20 h, until the reaction solution was yellowish with iron and blue or green with cobalt. Any solid material formed during the reduction was filtered off and the filtrate was placed in a 100 mL round-bottom vessel. The solution was concentrated to dryness and the residue dissolved in CH_2Cl_2. The products were crystallized as described above.

All of the reactions produced a mixture of products with variable ratios depending on the reaction time and conditions. In the cases of complexes **1**, **2**, **3**, **8** and **11**, the yields were very low and varied

Table 2. Crystallographic data for **1**–**2**.

	1	**2a**	**2b**	**2c**
Empirical formula	$C_{10}H_{12}Cl_6CoO_8Ru_2$	$C_6H_4Cl_6CoO_8Ru_2$	$C_6H_4Cl_6CoO_8Ru_2$	$C_6H_4Cl_6CoO_8Ru_2$
Formula mass	733.97	677.86	677.86	677.86
Temperature [K]	100(2)	120(2)	150(2)	150(2)
λ [Å]	0.71073	0.71073	0.71073	0.71073
Crystal system	monoclinic	monoclinic	triclinic	monoclinic
Space group	$P2_1/c$	$P2_1/n$	$P\bar{1}$	$P2_1/c$
a [Å]	9.1922(3)	7.0428(15)	6.3339(2)	10.1061(3)
b [Å]	10.9226(3)	15.489(3)	10.4649(3)	6.3789(2)
c [Å]	11.0099(4)	8.4505(15)	14.3176(5)	27.6699(9)
α [°]	90	90	87.315(2)	90
β [°]	96.482(2)	96.808(15)	81.818(2)	95.5550(10)
γ [°]	90	90	74.300(2)	90
V [Å^3]	1098.36(6)	915.3(3)	904.28(5)	1775.39(10)
Z	2	2	2	4
$\rho_{calcd.}$ [Mg/m^3]	2.219	2.459	2.490 Mg/m^3	2.536
μ(Mo-K_a) [mm^{-1}]	2.866	3.428	3.470 mm^{-1}	3.535
No. of reflections	22720	8499	6593	8861
Unique reflections	2499	2090	4070	3797
R_{int}	0.0580	0.0564	0.0256	0.0342
R_1[a] ($I \geq 2\sigma$)	0.0245	0.0309	0.0289	0.0294
wR_2[b] ($I \geq 2\sigma$)	0.0571	0.0507	0.0601	0.0511

[a] $R_1 = \Sigma||F_o| - |F_c||/\Sigma|F_o|$. [b] $wR_2 = \{\Sigma[w(F_o^2 - F_c^2)^2]/\Sigma[w(F_o^2)^2]\}^{1/2}$.

from reaction to reaction. In these cases the identification of the products was based on single-crystal X-ray analysis.

Analysis of Separated and Purified Complexes 1–3, 8 and 11

$[Ru_2Cl_2(\mu\text{-}Cl)_4(CO)_6Co(CH_3CH_2OH)_2]$ (1): $C_{10}H_{12}Cl_6CoO_8Ru_2$ (733.99): calcd. C 16.36, H 1.65; found C 16.24, H 1.69. ATR-IR $\tilde{\nu}$(CO) = 2137 (vs), 2075 (vs), 2054 cm^{-1} (vs). Yield: 10–15%.

$[Ru_2Cl_2(\mu\text{-}Cl)_4(CO)_6Co(H_2O)_2]\cdot(H_2O)$ (2): $C_6H_6Cl_6CoO_9Ru_2$ (695.90): calcd. C 10.36, H 0.87; found C 10.11, H 0.97. ATR-IR $\tilde{\nu}$(CO) = 2135 (vs), 2070 (vs), 2054 cm^{-1} (vs). Yield: 8%.

$[RuCl_3(CO)_3]_2[Co(H_2O)_6]\cdot(H_2O)$ (3): $C_6H_{14}Cl_6CoO_{13}Ru_2$ (767.96): calcd. C 9.38, H 1.84; found 9.34, H 2.01. ATR-IR $\tilde{\nu}$(CO) = 2139 (vs), 2075 (vs), 2056 cm^{-1} (vs). Yield: 16%.

$[OsCl_3(CO)_3]_2[Co(H_2O)_6]$ (8): $C_6H_{12}Cl_6CoO_{12}Os_2$ (928.21): calcd. C 7.76, H 1.30; found C 7.70, H 1.31. ATR-IR $\tilde{\nu}$(CO) = 2126 (vs), 2043 (vs), 2024 cm^{-1} (vs). Yield: 24%.

$[RuI_2(CO)_3]_2$ (11): $C_{60}I_4O_6Ru_2$ (877.82): calcd. C 8.21; found C 8.21. IR (CH_2Cl_2): $\tilde{\nu}$(CO) = 2118 (s) , 2055 (sh, s) cm^{-1}.

X-ray Crystal Structure Determinations: The crystals were immersed in cryo-oil, mounted in a Nylon loop and measured at a temperature of 100–150 K. The X-ray diffraction data was collected by means of a Nonius KappaCCD diffractometer using Mo-K_α radiation (λ = 0.71073 Å). The Denzo-Scalepack[25] or EvalCCD[26] program packages were used for cell refinements and data reductions. The structures were solved by direct methods or by the heavy-atom method using SHELXS-97,[27] SIR-97,[28] or

Table 3. Crystallographic data for **3**–**6**.

	3	**4**	**5**	**6**
Empirical formula	$C_6H_{16}Cl_6CoO_{14}Ru_2$	$C_6H_{16}FeI_6O_{14}Ru_2$	$C_6H_{16}CoI_6O_{14}Ru_2$	$C_6H_{12}Cl_6FeO_{12}Os_2$
Formula mass	785.96	1331.58	1334.66	925.11
Temperature [K]	100(2)	100(2)	110(2)	120(2)
λ [Å]	0.71073	0.71073	0.71073	0.71073
Crystal system	triclinic	monoclinic	monoclinic	triclinic
Space group	$P\bar{1}$	$P2_1/c$	$P2_1/c$	$P\bar{1}$
a [Å]	6.2044(3)	12.6166(2)	12.6371(4)	6.2890(14)
b [Å]	7.1225(2)	9.5667(2)	9.5821(3)	6.3520(10)
c [Å]	14.7970(7)	12.4005(2)	12.4173(5)	13.939(3)
α [°]	91.603(3)	90	90	87.901(7)
β [°]	98.438(2)	109.3620(10)	109.3740(10)	77.217(5)
γ [°]	115.186(3)	90	90	80.630(7)
V [Å^3]	582.33(5)	1412.08(4)	1418.47(9)	535.8(2)
Z	1	2	2	1
$\rho_{calcd.}$ [Mg/m^3]	2.241	3.132	3.125	2.867
μ(Mo-K_α) [mm^{-1}]	2.729	8.170	8.207	13.293
No. of reflections	8390	9461	12152	6598
Unique reflections	2634	3177	3217	1840
R_{int}	0.0241	0.0606	0.0408	0.0820
R_1[a] ($I \geq 2\sigma$)	0.0219	0.0333	0.0242	0.0523
wR_2[b] ($I \geq 2\sigma$)	0.0536	0.0791	0.0582	0.1215

[a] $R_1 = \Sigma||F_o| - |F_c||/\Sigma|F_o|$. [b] $wR_2 = \{\Sigma[w(F_o^2 - F_c^2)^2]/\Sigma[w(F_o^2)^2]\}^{1/2}$.

Table 4. Crystallographic data for **7**–**9**.

	7	**8a**	**8b**	**9**
Empirical formula	$C_3H_{12}Cl_5FeO_9Os$	$C_6H_{16}Cl_6CoO_{14}Os_2$	$C_6H_{12}Cl_6CoO_{12}Os_2$	$C_{10}H_{12}Cl_6CoO_8Os_2$
Formula mass	615.43	964.22	928.19	912.23
Temperature[K]	120(2)	120(2)	120(2)	120(2)
λ [Å]	0.71073	0.71073	0.71073	0.71073
Crystal system	monoclinic	triclinic	triclinic	monoclinic
Space group	$P2_1/n$	$P\bar{1}$	$P\bar{1}$	$P2_1/c$
a [Å]	11.7840(12)	6.2144(2)	6.2750(12)	9.1912(5)
b [Å]	9.4780(11)	7.1074(2)	6.3310(13)	10.9224(6)
c [Å]	15.1490(11)	14.8771(6)	13.877(3)	11.0355(6)
α [°]	90	91.495(2)	87.455(11)	90
β [°]	108.032(6)	98.393(2)	77.067(11)	96.174(3)
γ [°]	90	115.275(2)	80.810(12)	90
V [Å^3]	1608.9(3)	584.95(3)	530.39(19)	1101.43(10)
Z	4	1	1	2
$\rho_{calcd.}$ [Mg/m^3]	2.541	2.737	2.906	2.751
μ(Mo-K_α) [mm^{-1}]	9.650	12.277	13.527	13.012
No. of reflections	11930	10546	6704	11536
Unique reflections	3663	2673	1824	2164
R_{int}	0.0474	0.0306	0.0788	0.0437
R_1[a] ($I \geq 2\sigma$)	0.0308	0.0231	0.0496	0.0319
wR_2[b] ($I \geq 2\sigma$)	0.0603	0.0517	0.1200	0.0693

[a] $R_1 = \Sigma||F_o| - |F_c||/\Sigma|F_o|$. [b] $wR_2 = \{\Sigma[w(F_o^2 - F_c^2)^2]/\Sigma[w(F_o^2)^2]\}^{1/2}$.

Table 5. Crystallographic data for **10**–**12**.

	10	**11**	**12**
Empirical formula	$C_5H_6Cl_2O_4Os$	$C_6I_4O_6Ru_2$	$C_4I_2O_4Ru$
Formula mass	391.20	877.80	466.91
Temperature [K]	120(2) K	100(2)	110(2)
λ [Å]	0.71073 Å	0.71073	0.71073
Crystal system	Monoclinic	Monoclinic	Monoclinic
Space group	$P2_1/n$	$C2/m$	$C2/c$
a [Å]	6.0129(5)	11.0765(4)	7.1062(3)
b [Å]	16.5884(8)	7.6845(3)	10.9172(4)
c [Å]	9.7260(4)	9.6081(4)	12.5486(3)
α [°]	90	90	90°
β [°]	96.584(5)	107.759(2)	92.399(3)°
γ [°]	90	90	90
V [Å^3]	963.72(10)	778.85(5)	972.66(6)
Z	4	2	4
$\rho_{calcd.}$ [Mg/m^3]	2.696	3.743	3.188
μ(Mo-K_α) [mm^{-1}]	13.758	9.877	7.927
No. of reflections	7892	4707	4190
Unique reflections	2197	832	952
R_{int}	0.0469	0.0284	0.0228
R_1[a] ($I \geq 2\sigma$)	0.0274	0.0132	0.0180
wR_2[b] ($I \geq 2\sigma$)	0.0379	0.0282	0.0336

[a] $R_1 = \Sigma||F_o| - |F_c||/\Sigma|F_o|$. [b] $wR_2 = \{\Sigma[w(F_o^2 - F_c^2)^2]/\Sigma[w(F_o^2)^2]\}^{1/2}$.

Table 6. Selected bond lengths [Å] and bond angles [°] of the complexes **1**, **2a**, **2b**, **3**, **4**, presented in Figures 4, 5, 6, and 7.

Bond length [Å]	**1**	**2a**	**2b**	**3**	**4**
C1–M1	1.900(3)	1.909(4)	1.916(3)	1.907(2)	1.913(6)
C2–M1	1.916(3)	1.899(5)	1.8994	1.921(2)	1.908(6)
C3–M1	1.908(3)	1.901(4)	1.904(3)	1.901(2)	1.916(6)
C4–M2			1.911(4)		
C5–M2			1.908(3)		
C6–M2			1.911(4)		
X1–M1	2.4208(6)	2.4251(10)	2.4166(7)	2.4239(5)	2.7441(5)
X2–M1	2.4275(6)	2.4083(11)	2.4221(9)	2.4105(5)	2.7471(5)
X3–M1	2.4186(6)	2.4129(11)	2.4154(8)	2.4275(6)	2.7357(5)
O4–M1					
X4–M2			2.4082(8)		
X5–M2			2.4284(8)		
X6–M2			2.4120(9)		
X1–M′1	2.4844(6)		2.4876(10)		
X2–M′1	2.5172(6)		2.4646(8)		
X4–M′1			2.4353(8)		
X5–M′1			2.4711(9)		
O4–M′1		2.053(3)		2.0823(16)	2.142(4)
O5–M′1				2.0775(16)	2.077(4)
O6–M′1				2.0988(16)	2.132(4)
O7–M′1			2.057(3)		
O8–M′1			2.019(2)		
Bond angle [°]	**1**	**2a**	**2b**	**3**	**4**
C1–M1–C2	91.45(11)	91.4(2)	92.07(14)	93.40(9)	93.4(2)
C1–M1–X1					
C1–M1–C3					
C5–M2–C6			92.32(15)		
C3–M1–X3	179.15(8)	176.85(12)	178.89(11)	174.92(7)	177.5(2)
C4–M2–X4			176.44(10)		
C3–M1–O4					
X1–M1–X2	84.95(2)	86.18(3)	85.28(3)	90.76(2)	
X4–Ru2–X5			87.15(3)		
O4–M′1–X1	90.61(5)				
O4–M′1–X2	92.02(5)				
X1–M′1–X2	81.77(2)	84.76(3)	82.89(3)		92.010(16)
X4–M′1–X5			85.61(3)		
O4–M′1–O5				90.88(6)	87.40(15)
O4–M′1–O6				92.16(7)	87.57(15)
O5–M′1–O6				89.68(7)	89.97(14)
O8–M′1–O7			87.32(10)		
C1(A)–M1–C1					
X1(B)–M1–X1					

SIR2004[29] with a WinGX[30] graphical user interface. An empirical absorption correction was applied to all of the data (XPREP in SHELXTL v.6.14–1[31] or SADABS v.2.10[32]). Structural refinements were carried out using SHELXL-97.[33] In **1**, **2a**, **2c**, **3**, **4**, **5**, **7**, **8a**, **9** and **10** the H_2O and OH hydrogen atoms were located from the difference Fourier map but constrained to ride on their parent atom with U_{iso} = 1.5 U_{iso}(parent atom). In **2b** the H_2O hydrogen atoms were also located from the difference Fourier map and refined with fixed coordinates and fixed U_{iso} = 0.05. In **6** and **8b** the idealized positions of the H_2O hydrogen atoms were estimated using the HYDROGEN[34] program and they were constrained to ride on their parent atom by means of U_{iso} = 1.5 U_{iso}(parent atom). Other hydrogen atoms were positioned geometrically and were also constrained to ride on their parent atoms by means of C–H 0.98–0.99 Å and U_{iso} = 1.2–1.5 U_{iso}(parent atom). The structure of **12** is known and has been previously published in the early 1960s by Dahl and Wampler.[35] The crystallographic details are summarized in Tables 2, 3, 4 and 5. The thermal ellipsoid plots and selected bond lengths and angles for structures **1**, **2a**, **3**, **4**, **8a** and **9**–**12** are given in Figures 3, 4, 5, 6, 7, 8, 9, 10, 11, and 12 and Tables 6 and 7; for the other structures, see the Supporting Information. CCDC-630761 to -630775 (**1**–**12**, respectively) contain the supplementary

Table 7. Selected bond lengths [Å] and bond angles [°] of the complexes **8a** and **9**–**12** presented in Figures 8, 9, 10, 11, and 12.

Bond length [Å]	**8a**	**9**	**10**	**11**	**12**
C1–M1	1.897(5)	1.905(10)	1.909(5)	1.907(3)	1.933(4)
C2–M1	1.902(5)	1.896(8)	1.892(5)		
C3–M1	1.918(5)	1.912(9)	1.896(6)	1.933(4)	1.982(4)
C4–M2					
C5–M2					
C6–M2					
X1–M1	2.4359(10)	2.436(2)	2.3908(12)	2.7292(3)	2.7332(4)
X2–M1	2.4329(10)	2.429(2)	2.4154(12)		
X3–M1	2.4165(10)	2.424(2)		2.7355(4)	
O4–M1			2.133(3)		
X4–M2					
X5–M2					
X6–M2					
X1–M′1		2.514(2)			
X2–M′1		2.486(2)			
X4–M′1					
X5–M′1					
O4–M′1	2.078(3)	1.996(6)			
O5–M′1	2.107(3)				
O6–M′1	2.080(3)				
O7–M′1					
O8–M′1					
Bond angle [°]	**8a**	**9**	**10**	**11**	**12**
C1–M1–C2	92.1(2)	91.2(4)	92.3(2)		
C1–M1–X1					178.68(12)
C1–M1–C3					92.90(16)
C5–M2–C6					
C3–M1–X3	177.05(13)	178.7(2)		178.36(11)	
C4–M2–X4					
C3–M1–O4			173.75(15)		
X1–M1–X2	87.53(3)	81.22(6)	88.13(4)		
X4–Ru2–X5					
O4–M′1–X1					
O4–M′1–X2					
X1–M′1–X2					
X4–M′1–X5					
O4–M′1–O5	90.26(12)				
O4–M′1–O6	89.58(12)				
O5–M′1–O6	92.11(13)				
O8–M′1–O7					
C1(A)–M1–C1				95.46(15)	
X1(B)–M1–X1				85.632(11)	

crystallographic data for this paper. These data can be obtained free of charge from The Cambridge Crystallographic Data Centre via www.ccdc.cam.ac.uk/data_request/cif.

Computational Work: Full geometry optimization of the complexes was performed using the DFT method with a non-local hybrid functional B3PW91. The Stuttgart-Dresden ECP basis set was used for the metals (Fe, Co, Ru and Os)[36] and 6-31G* for others (C, H, O and Cl). The calculations were made with the Gaussian03 program package.[37]

Supporting Information (see footnote on the first page of this article): Figures S1–S5: Thermal ellipsoid plots (at 50% probability level) of **2c**, **5**, **6**, **7**, **8a** and **10**; Figures S6 and S7: ATR-IR spectra of complexes **1**, **2**, **3** and **8**.

Acknowledgments

Financial support in the form of a grant (grant no. 210265) provided by the Academy of Finland is gratefully acknowledged. The authors would also like to thank Dr. Sari Suvanto for the EDS and ATR measurements, Ritva Romppanen for the elemental analysis measurements, and Dr. Larisa Oresmaa for her valuable comments.

[1] a) R. Brittain, A. L. Hickman, *Brit. UK Pat. Appl.* 20504727 19810107, **1981**; b) L. Bertolini, M. Gastaldi, M. P. Pedeferri, E. Redaelli, *Corros. Sci.* **2002**, *44*, 1497–1513; c) S. Paul, K. Basu, P. Mitra, *Bull. Electrochem.* **2005**, *21*, 269–273; d) G. Glass, *PCT Int. Appl.* WO 2006003473, **2006**.

[2] a) A. M. Vecchio-Sadus, *J. Appl. Electrochem.* **1993**, *23*, 401–416; b) M. T. Reetz, M. Winter, R. Breinbauer, T. Thurn-Albrecht, W. Vogel, *Chem. Eur. J.* **2001**, *7*, 1084–1094.

[3] A. Shantaram, H. Beyenal, R. R. A. Veluchamy, Z. Lewandowski, *Environ. Sci. Technol.* **2005**, *39*, 5037–5042.

[4] a) M. A. Méndez-Rojas, F. Cordova-Lozano, G. Gojon-Zorilla, E. González-Vergara, M. A. Quiroz, *Polyhedron* **1999**, *18*, 2651–2658; b) B. I. Kharisov, L. M. Blanco, A. D. Garnovskii, A. S. Burlov, L. I. Kuznetsova, L. V. Korovina, D. A. Garnovskii, T. Dieck, *Polyhedron* **1998**, *17*, 381–389; c) J. M. Paratian, E. Labbé, S. Sibile, J. Y. Nédélec, J. Périchon, *J. Organomet. Chem.* **1995**, *487*, 61–64; d) J. Sánchez-Piso, A. Carcía-Vázquez, J. Romero, M. L. Durán, A. Sousa-Pedras, E. Labisbal, O. R. Nascimento, *Inorg. Chim. Acta* **2002**, *328*, 111–122; e) H. Fillon, C. Gosmini, J.-Y. Nédélec, J. Périchon, *Tetrahedron Lett.* **2001**, *42*, 3843–3846.

[5] J. Castro, S. Cabaleiro, P. Pérez-Lourido, J. Romero, J. A. Garcia-Vásquez, A. Sousa, *Z. Anorg. Allg. Chem.* **2002**, *628*, 1210–1217.

[6] a) M. Faticanti, N. Cioffi, S. De Rossi, N. Ditaranto, P. Porta, L. Sabbatini, T. Bleve-Zacheo, *Appl. Catal., B* **2005**, *60*, 73–82; b) N. Cioffi, N. Ditaranto, L. Torsi, R. A. Picca, E. De Giglio, L. Sabbatini, L. Novello, G. Tantillo, T. Bleve-Zacheo, P. G. Zambonin, *Anal. Bioanal. Chem.* **2005**, *382*, 1912–1918.

[7] a) E. Duñach, S. Dérien, J. Périchon, *J. Organomet. Chem.* **1989**, *364*, C33–C36; b) C. Moreau, F. Serein-Spirau, M. Bordeau, C. Biran, *J. Organomet. Chem.* **1998**, *570*, 147–154; c) T.-Y. Lin, T.-C. Chou, *J. Appl. Electrochem.* **1999**, *29*, 489–496; d) C. Gosmini, J. Y. Nédélec, J. Périchon, *Tetrahedron Lett.* **2000**, *41*, 5039–5042; e) A. A. Isse, A. Gennaro, *J. Electrochem. Soc.* **2002**, *149*, D113–D117; f) A. Palma, B. A. Frontana-Uribe, J. Cárdenas, M. Saloma, *Electrochem. Commun.* **2003**, *5*, 455–459; g) H. Lund, H. Svith, S. U. Pedersen, K. Daasbjerg, *Electrochim. Acta* **2005**, *51*, 655–664; h) O. Scialdone, A. Galia, C. La Rocca, G. Filardo, *Electrochim. Acta* **2005**, *50*, 3231–3242.

[8] L. Mond, C. Langer, F. Quincke, *J. Chem. Soc. Trans.* **1890**, *57*, 749–753.

[9] M. Haukka, M. Jakonen, N. Nivajärvi, M. Kallinen, *Dalton Trans.* **2006**, 3212–3220.

[10] J. Chatt, B. L. Shaw, A. E. Field, *Chem. Ind.* **1964**, 3466–3475, and ref.[1] cited therein.

[11] M. L. Berch, A. Davison, *J. Inorg. Nucl. Chem.* **1973**, *35*, 3763–3767.

[12] C. R. Eady, P. F. Jackson, B. F. G. Johnson, J. Lewis, M. C. Malatesta, *J. Chem. Soc. Dalton Trans.* **1980**, 383–392.

[13] A. J. Deeming, M. Karim, *Polyhedron* **1991**, *10*, 837–840.

[14] H. A. Mirza, J. J. Vittal, R. J. Puddephatt, *Inorg. Chem.* **1993**, *32*, 1327–1332.

[15] E. Lucenti, E. Cariati, C. Dragonetti, D. Roberto, *J. Organomet. Chem.* **2003**, *669*, 44–47.

[16] M. Fauré, L. Maurette, B. Donnadieu, G. Lavigne, *Angew. Chem. Int. Ed.* **1999**, *38*, 518–522.

[17] M. Fauré, C. Saccavini, G. Lavigne, *Chem. Commun.* **2003**, 1578–1579.

[18] J. P. Collman, W. R. Roper, *J. Am. Chem. Soc.* **1966**, *88*, 3504–3508.

[19] M. Aracama, M. A. Esteruelas, F. J. Lahoz, J. A. Lopez, U. Meyer, L. A. Oro, H. Werner, *Inorg. Chem.* **1991**, *30*, 288–293.

[20] S. Dev, J. P. Selegue, *J. Organomet. Chem.* **1994**, *469*, 107–110.

[21] a) D. Roberto, R. Psaro, R. Ugo, *Organometallics* **1993**, *12*, 2292–2296; b) D. Roberto, R. Psaro, R. Ugo, *J. Mol. Catal.* **1994**, *86*, 109–120; c) E. Lucenti, D. Roberto, R. Ugo, *Organometallics* **2001**, *20*, 1725–1733; d) D. Roberto, E. Cariati, R. Psaro, R. Ugo, *Organometallics* **1994**, *13*, 734–737; e) D. Roberto, E. Cariati, R. Ugo, R. Psaro, *Inorg. Chem.* **1996**, *35*, 2311–2316; f) D. Roberto, E. Cariati, E. Lucenti, M. Respini, R. Ugo, *Organometallics* **1997**, *16*, 4531–4539; g) C. Roveda, E. Cariati, E. Lucenti, D. Roberto, *J. Organomet. Chem.* **1999**, *580*, 117–127.

[22] H. H. Uhlig, R. W. Revie, *Corrosion and Corrosion Control, An Introduction to Corrosion Science and Engineering*, 3rd ed., John Wiley & Sons, New York, **1985**, p. 78–87 and references cited therein.

[23] P. Hirva, M. Haukka, M. Jakonen, T. A. Pakkanen, *Inorg. Chim. Acta* **2006**, *359*, 853–862.

[24] M. I. Bruce, C. M. Jensen, N. L. Jones, *Inorg. Synth.* **1989**, *26*, 259–261.

[25] Z. Otwinowski, W. Minor, in *Methods in Enzymology*, vol. 276 ("Macromolecular Crystallography"), part A (Eds.: C. W. Carter, J. Sweet), Academic Press, New York, USA, **1997**, pp. 307–326.

[26] A. J. M. Duisenberg, L. M. J. Kroon-Batenburg, A. M. M. Schreurs, *J. Appl. Crystallogr.* **2003**, *36*, 220–229.

[27] G. M. Sheldrick, *SHELXS-97, Program for Crystal Structure Determination, University of Göttingen*, Göttingen, Germany, **1997**.

[28] A. Altomare, M. C. Burla, M. C. Camalli, C. Giacovazzo, A. Guagliardi, A. G. G. Moliterni, G. Polidori, R. Spagna, *J. Appl. Crystallogr.* **1999**, *32*, 115–119.

[29] M. C. Burla, M. Camalli, B. Carrozzini, G. L. Cascarano, C. Giacovazzo, G. Polidori, R. Spagna, *J. Appl. Crystallogr.* **2005**, *38*, 381–388.

[30] L. J. Farrugia, *J. Appl. Crystallogr.* **1999**, *32*, 837.

[31] G. M. Sheldrick, *SHELXTL*, v. 6.14-1, Bruker Analytical X-ray Systems, Bruker AXS, Inc., Madison, Wisconsin, USA, **2005**.

[32] G. M. Sheldrick, *SADABS, Bruker Nonius scaling and absorption correction*, v. 2.10, Bruker AXS, Inc., Madison, Wisconsin, USA, **2003**.

[33] G. M. Sheldrick, *SHELXL-97, Program for Crystal Structure Refinement*, University of Göttingen, Göttingen, Germany, **1997**.

[34] M. Nardelli, *J. Appl. Crystallogr.* **1999**, *32*, 563–571.

[35] L. F. Dahl, D. F. Wampler, *Acta Crystallogr.* **1962**, *15*, 946–950.

[36] The basis set was obtained from the Extensible Computational Chemistry Environment Basis Set Database, version 9/12/01,

as developed and distributed by the Molecular Science Computing Facility, Environmental and Molecular Sciences Laboratory, which is part of the Pacific Northwest Laboratory, P. O. Box 999, Richland, Washington 99352, USA, and funded by the U. S. Department of Energy. The Pacific Northwest Laboratory is a multi-program laboratory operated by the Battelle Memorial Institute for the U. S. Department of Energy under contract DE-AC06-76RLO 1830. Contact David Feller or Karen Schuchardt for further information.

[37] M. J. Frisch, G. W. Trucks, H. B. Schlegel, G. E. Scuseria, M. A. Robb, J. R. Cheeseman, J. A. Montgomery, Jr., T. Vreven, K. N. Kudin, J. C. Burant, J. M. Millam, S. S. Iyengar, J. Tomasi, V. Barone, B. Mennucci, M. Cossi, G. Scalmani, N. Rega, G. A. Petersson, H. Nakatsuji, M. Hada, M. Ehara, K. Toyota, R. Fukuda, J. Hasegawa, M. Ishida, T. Nakajima, Y. Honda, O. Kitao, H. Nakai, M. Klene, X. Li, J. E. Knox, H. P. Hratchian, J. B. Cross, V. Bakken, C. Adamo, J. Jaramillo, R. Gomperts, R. E. Stratmann, O. Yazyev, A. J. Austin, R. Cammi, C. Pomelli, J. W. Ochterski, P. Y. Ayala, K. Morokuma, G. A. Voth, P. Salvador, J. J. Dannenberg, V. G. Zakrzewski, S. Dapprich, A. D. Daniels, M. C. Strain, O. Farkas, D. K. Malick, A. D. Rabuck, K. Raghavachari, J. B. Foresman, J. V. Ortiz, Q. Cui, A. G. Baboul, S. Clifford, J. Cioslowski, B. B. Stefanov, G. Liu, A. Liashenko, P. Piskorz, I. Komaromi, R. L. Martin, D. J. Fox, T. Keith, M. A. Al-Laham, C. Y. Peng, A. Nanayakkara, M. Challacombe, P. M. W. Gill, B. Johnson, W. Chen, M. W. Wong, C. Gonzalez, J. A. Pople, *Gaussian 03*, revision C.02, Gaussian, Inc., Wallingford, CT, **2004**.

Received: March 27, 2007
Published Online: June 5, 2007

